Dissecting the heterogeneity of circulating and tissue-resident memory T cells

Gracht, E.T.I. van der

3

Boost immunization elicits diversification of circulating and tissue-resident CD8$^+$ memory T cells

Esmé T.I. van der Gracht[1]
Guillaume Beyrend[1]
Elham Beyranvand Nejad[1]
Tamim Abdelaal[2,3]
Felix M. Behr[1]
Thomas H. Wesselink[1]
Frits Koning[1]
Klaas P.J.M. van Gisbergen[4]
Ramon Arens[1]

Affiliations

[1]Department of Immunology, Leiden University Medical Center, 2333ZA, The Netherlands.
[2]Delft Bioinformatics Lab, Delft University of Technology, Delft, 2628XE, The Netherlands.
[3]Leiden Computational Biology Center, Leiden University Medical Center, Leiden 2333ZA, The Netherlands.
[4]Department of Hematopoiesis, Sanquin Research and Landsteiner Laboratory, Amsterdam, The Netherlands

Manuscript in preparation

Abstract

T cell-mediated immune responses play crucial roles in protection against infection and malignant disease. Repetitive immunization by prime-boost vaccination or pathogen re-encounter increases memory T cell numbers and generates long-term protective T-cell responses. The impact of recurring antigen stimulation on the differentiation of circulating and tissue-resident $CD8^+$ T cell populations is however not fully understood. Here, we show that second and third immunizations profoundly impacted the magnitude of antigen-specific memory $CD8^+$ T cells. Using high-dimensional single-cell mass cytometry we delineated that especially second immunizations sculps the heterogeneity of vaccine-induced $CD8^+$ T cells organ-wide. Moreover, by using lineage tracing of antigen-specific $CD8^+$ T cells, we show that the development of circulating $CD8^+$ ex-T_{RM} cells is most profoundly impacted by tertiary immunization. Together, these data show that repeated antigen triggering has a dynamic and profound impact on the magnitude and diversification of antigen-specific circulating and tissue-resident $CD8^+$ memory T cells organ-wide and is key in the development of protective prime-boost vaccination.

Introduction

T cell-mediated immune responses play critical roles in acquiring immunity against infections and malignant disease. Repetitive immunization, either by prime-boost vaccination or pathogen re-encounter, increases the number of memory T cells, and this concept has become increasingly evident in vaccine design. Importantly, the induction of durable T cell responses of sufficient magnitude and quality is key in vaccine-induced immunity (1, 2). In this respect, understanding the mechanisms of repetitive immunizations is critical to advance the development of T cell-based vaccines.

Homologous or heterologous booster vaccine regimens, where a second vaccine is administered after an indicated period of time, are used to acquire sufficient immunity against infectious disease (3, 4). Many vaccines in national vaccination programs require a booster vaccine, including vaccines against diphtheria, pertussis, hepatitis B and human papilloma virus (HPV) (5). Also for most vaccines against Covid-19, booster vaccines are highly recommended (6). Even though booster vaccination is commonly used to generate long-term protective immune response, the effect of boosting on the differentiation of heterogeneous memory $CD8^+$ T cell populations is not fully understood.

The increase in the number of circulating memory T cells upon booster immunization has been well documented, and recently this has also been observed for tissue-resident memory T (T_{RM}) cells, which are excluded from the blood circulation and reside in non-lymphoid tissues (7, 8). Moreover, also upon vaccination with adenoviral vectors that induce low level persistent antigen-triggering, both circulating as well as $CD8^+$ T_{RM} cells are increase in multiple tissues, and both are implicated in protection (9). Recently, it has also been observed that T_{RM} cells have the capacity to re-enter the circulation and shape systemic T cell responses upon re-challenge (10-12). However, the effect of antigen-triggering on the development of $CD8^+$ ex-T_{RM} remains incompletely understood.

Here, we studied the effect of antigen-triggering by booster synthetic long peptide (SLP) vaccinations focused on the diversification of vaccine-induced memory $CD8^+$ T cells. SLP vaccine platforms can be designed to induce exclusive $CD4^+$ or $CD8^+$ T cell responses against single or multiple epitopes present in pathogens and malignant cells. Clinically, SLP vaccines

are used as immunotherapy of pre-malignant disease and combined with other therapies are also active against established malignant disease (13, 14). To gain in-depth insight into the differentiation of the antigen-specific $CD8^+$ T cell phenotype in prime-boost settings we used high-dimensional mass cytometry with 41 markers including indicators for recognizing antigen-specific cells. Booster vaccination impacted both the magnitude and diversification of antigen-specific $CD8^+$ T_{CM}, T_{EM}, and T_{RM} cell subsets leading to increased protection. Especially T_{EM} and T_{RM} subsets were increased upon the first boost, while a second boost empowered the development of $CD8^+$ ex-T_{RM} cells. Thus, additional antigen triggering results in disparate impact on the differentiation of circulating and tissue-resident memory T cell subsets.

Materials and methods

Mice

Wild-type C57BL/6 mice were obtained from Charles River Laboratories (L'Arbresle, France) or Jackson Laboratory (Sacramento, CA, USA). CD45.1 Hobit reporter and CD45.2 Hobit reporter X ROSA26-eYFP LT mice were previously described and spleens were obtained from the group of Van Gisbergen, Sanquin (10). At the start of the experiments, mice were six to eight-week-old. Animals were housed in individually ventilated cages under specific-pathogen free conditions at the animal facility at the Leiden University Medical Center (LUMC). All animal experiments were approved by the Animal Experiments Committee of LUMC and performed according to the recommendations and guidelines set by LUMC and by the Dutch Experiments on Animals Act.

Peptide vaccination

GP34 synthetic long peptide (SLP) (sequence: KAVYNFATCGIFALIS), OVA SLP (sequence: SMLVLLPDEVSGLEQLESIINFEKLTEWTS) and E7 SLP (sequence: GQAEPDRAHYNIVTFCCKCDS) were produced at the peptide facility of the LUMC. The purity of the synthesized peptide (75–90%) was determined by HPLC and the molecular weight by mass spectrometry. Mice were vaccinated subcutaneously (s.c.) at the tail base with 100µg synthetic long peptide + 20µg CpG (ODN 1826, InvivoGen) dissolved in PBS. Booster vaccinations were provided with 2 weeks interval.

Viral and bacterial infections

MCMV-IE2 OVA and MCMV-M45 OVA were generated and reconstituted as described elsewhere (15, 16). In brief, nucleotide sequences encoding the SIINFEKL epitope of chicken ovalbumin were inserted by targeted mutagenesis at the C-terminus of the IE2 or M45 genes. Mice were infected intraperitoneally with $1x10^4$ infectious units (IU) MCMV-IE2 OVA or $1x10^4$ IU MCMV-M45 OVA. *Listeria monocytogenes* (LM) expressing OVA (LM-OVA) was previously described (17). In brief, LM-OVA contains a chromosomally integrated Ag cassette encoding truncated OVA (aa 134–387). Mice were infected intravenously via retro-orbital injection with $1x10^4$ colony-forming units (CFU) LM-OVA. To quantify the bacterial load in liver, livers were isolated and subsequently minced in PBS using 70 µm cell strainers. Dilution series were made in 0.1% Triton X-100 Lysis buffer after which they were plated on Brain Heart

Infusion (70138, Merck Millipore) agar plates. After 24 hours incubation at 37°C, bacterial colonies were quantified.

Tumor challenge

The TC-1 tumor cell line (a kind gift from T.C. Wu, John Hopkins University, Baltimore, MD) was developed by retroviral transduction of C57BL/6 lung epithelial cells with the HPV16 E6/E7 and c-H-ras oncogenes (18). Mice were inoculated subcutaneously in the flank with 1×10^5 TC-1 tumor cells. Tumor size (mm3) was measured two times a week using a caliper and calculated as (L×W×H)×0.52 (L: length, W: width, H: height). Mice were euthanized when tumor size reached 500-1000 mm3 in volume. Mycoplasma tests were frequently performed by PCR and were negative for all cell lines. Cell lines were authenticated with a microsatellite PCR.

Isolation of T cells

Peripheral blood was collected from the tail vein. Splenocytes were obtained by mincing the tissue through cell strainers. Bone-marrow cells were obtained from the femurs and tibias by centrifugation. Blood cells, splenocytes and bone marrow cells were depleted of erythrocytes using ammonium chloride lysis buffer. Subsequently, bone-marrow T cells were isolated using MicroBeads (130-095-130, Miltenyi Biotec) according to manufacturers' protocol.

To remove remaining circulating blood cells from the liver and lungs, mice were perfused with 20 ml PBS containing 2 mM EDTA. Next, liver and lungs were cut into small pieces using surgical knives. Liver tissue was resuspended in 3.5 ml IMDM containing 250 U/ml collagenase type 1-A (C2674, Sigma) and 20 µg/ml DNase I (D5025, Sigma), and lung tissue was incubated with 1 ml IMDM and 250 U/ml collagenase and 20 µg/ml DNase. After incubation with collagenase/DNase for 25 minutes at 37°C, liver and lung tissue were dissociated into single-cell suspensions using 70 µm cell strainers, and subsequently lymphocytes were isolated using a Percoll (GE Healthcare) gradient.

Adoptive T cell transfers

Spleens of CD45.1 Hobit reporter OT-1 or CD45.2 Hobit reporter x ROSA26-eYFP LT mice were isolated and subsequently $CD8^+$ T cells were isolated by negative selection using MicroBeads (130-104-075, Miltenyi Biotec) according to the manufacturer's protocol. Splenic $CD8^+$ T cells were adoptively transferred via retro-orbital injection into naïve Ly5.2 mice.

Flow cytometry

Fluorescently labelled monoclonal antibodies against the following mouse antigens were used: CD3 (clone 145-2C11, BD Biosciences), CD4 (clone RM4-5, BioLegend), CD8 (clone 53-6.7, BioLegend), CD127 (clone A7R34, ThermoFisher), KLRG1 (clone 2F1, ThermoFisher), CD44 (clone IM7, BioLegend), CD62L (clone MEL-14, BioLegend), CD69 (clone H1.2F3, BD Biosciences), CD38 (clone 90, Thermo Fisher), CX3CR1 (clone SA011F11, Biolegend), CD11c (clone HL3, BD Biosciences), Sca-1 (clone D7, Biolegend). 7-AAD (A1310, Invitrogen) staining was used to exclude dead cells. Cells were stained according to our previously published protocol (9). GP34-specific, OVA-specific or E7-specific $CD8^+$ T cells were quantified using MHC class I tetramers for the peptide epitopes $GP_{34\text{-}41}$ (AVYNFATC), $OVA_{257–264}$ (SIINFEKL), HPV $E7_{49–57}$ (RAHYNIVTF) respectively. The presence of GP33-specific $CD8^+$ T cell responses was excluded using MHC class I tetramers for the epitope $GP_{33\text{-}41}$ (KAVYNFATC). Flow cytometric acquisition was performed on a BD Fortessa flow cytometer (BD Biosciences).

Mass cytometry

Metal-conjugated antibodies were either purchased from Fluidigm or were generated by conjugation of lanthanide metal isotopes to anti-mouse antibodies using the Maxpar X8 Polymer method according to the manufacturer's protocol (Fluidigm). Cisplatins 194 and 198 and Bismuth 209 were conjugated to anti-mouse monoclonal antibodies using protocols previously described (19, 20). All in-house conjugated antibodies were diluted to 0.5 mg/ml in antibody stabilizer supplemented with 0.05% sodium azide (Candor Biosciences). Serial dilution staining was performed on mouse lymphocytes to determine appropriate antibody dilution.

The CyTOF staining was performed as described elsewhere (21). In brief, around $3x10^6$ cells per sample were stained for CyTOF analysis. First, cells were stained in FACS buffer with PE and APC labelled tetramers and incubated for 30 minutes on ice. Cells were washed with Maxpar Cell Staining buffer (201068, Fluidigm) and subsequently incubated for 20 minutes with 1 µM Interchalator-Rh (201103A, Fluidigm) in staining buffer. Next, a-specific binding was prevented by incubating cells with Fc blocking solution and mouse serum for 15 minutes. Anti-PE and anti-APC were added in a final concentration of 1:50 and incubated for 45 minutes. The antibody mix was added and incubated for an additional 45 minutes. After washing the cells, samples were incubated overnight with 25nM Intercalator-Ir (201192A,

Fluidigm) in Maxpar Fix and Perm Buffer (201067, Fluidigm). Cells were pelleted in staining buffer and measured within one week. Before measuring, EQ™ Four Element Calibration Beads (201078, Fluidigm) were added in a 1:10 ratio.

Data analysis and statistics

Mass cytometry data analysis focused on the antigen-specific $CD8^+$ T cells. For the selection, we set our gating strategy to live single cells, positive for CD45, and excluded reference beads. The live $CD45^+$ gated files were compensated using Catalyst (22). Subsequently, MHC class I tetramer-specific $CD8^+$ T cells were selected in FlowJo for subsequent analysis.

Next, marker expression was ArcSinh5 transformed and subjected to dimensionality reduction analyses in Cytosplore (23) or FlowSOM (24). Cytoslore and FlowSOM were used for the identification of the clusters. For Cytosplore analysis, samples were analysed by hierarchical stochastic neighbourhood embedding (HSNE) (25) based on approximated t-distributed stochastic neighbourhood embedding (A-tSNE) (26). The similarity between tSNE maps was quantified using the Jensen-Shannon (JS) divergence as previously described (21). The JS divergence values ranged from 0 (indicating identical distributions) to 1 (indicating disjoint distributions). The dual tSNE analysis was performed to quantify the individual samples similarity based on the clusters composition as previously described (21, 27).

FlowSOM was used for the identification of vaccination and tissue-specific clusters. Using FlowSOM, 14 clusters were identified per analysis. Subsequently, Cytofast (28) was used for visualization and quantification of cell clusters. T_{RM} ($CD62L^-$ $CD69^+$), T_{CM} ($CD62L^+$ $CD69^-$) and T_{EM} ($CD62L^-CD69^-$) $CD8^+$ T cell clusters were selected by expression of CD69 and CD62L. Visualization of heatmaps and selection of clusters based on the size of the cluster (abundance of at least >5% of total) and significance was performed as previously described (21).

Statistical analyses were performed using Cytofast or GraphPad Prism (La Jolla, CA, Unites States). One-way ANOVA and log-rank (Mantel-Cox) survival test were used for statistical analysis. All P values were two-sided, and $P < 0.05$ was considered statistically significant.

Results

Prime-boost vaccination impacts the heterogeneity of circulating CD8+ T cells

To investigate the effect of antigen-triggering on the development and heterogeneity of CD8+ T cells, mice were vaccinated subcutaneously with synthetic long peptide (SLP) vaccines in a prime-boost-boost setting. We performed these experiments with SLP vaccines containing the class I restricted GP_{34-41} epitope from lymphocytic choriomeningitis virus (LCMV), or the class I restricted $E7_{49-57}$ epitope from human papilloma virus (HPV). The SLP vaccines were administered subcutaneously in prime-boost settings with 2 week intervals (prime only, prime-boost, prime-boost-boost) (**Figure 1A**). For both GP34 SLP and E7 SLP vaccines, a single immunization resulted in expansion of the antigen-specific CD8+ T cells that peaked to ~5% of the total CD8+ T cells around day 7 post-vaccination, followed by contraction and memory formation (**Figure 1B and S1A**). Booster immunization (2nd vaccine) increased the antigen-specific CD8+ T cell in the circulation, resulting in a higher maintenance of the antigen-specific memory CD8+ T cell population. Remarkably, after the second boost (3rd vaccine), a relatively higher level of the antigen-specific memory CD8+ T cell population in blood was observed as compared to the first booster. Flow cytometric analysis of the GP34-specific and E7-specific CD8+ T cells showed that the majority of these cells had a effector-memory phenotype based on the markers CD44 and KLRG1, that increased upon boosting (**Figure 1C**). Detailed analysis of memory CD8+ T cell differentiation by Cytosplore (23), which incorporates approximated t-distributed stochastic neighbourhood embedding (A-tSNE) algorithms for subset definition, revealed however a difference in the heterogeneity of the GP34-specific CD8+ T cells in blood at both the acute and memory phase of vaccination (**Figure 1D and 1E**). Phenotypical changes of antigen-specific CD8+ T cells occur gradually over time while differences in the phenotype change deeply upon sequential boosting. Thus, second and third immunization profoundly impact the magnitude and differentiation of circulating antigen-specific CD8+ T cells.

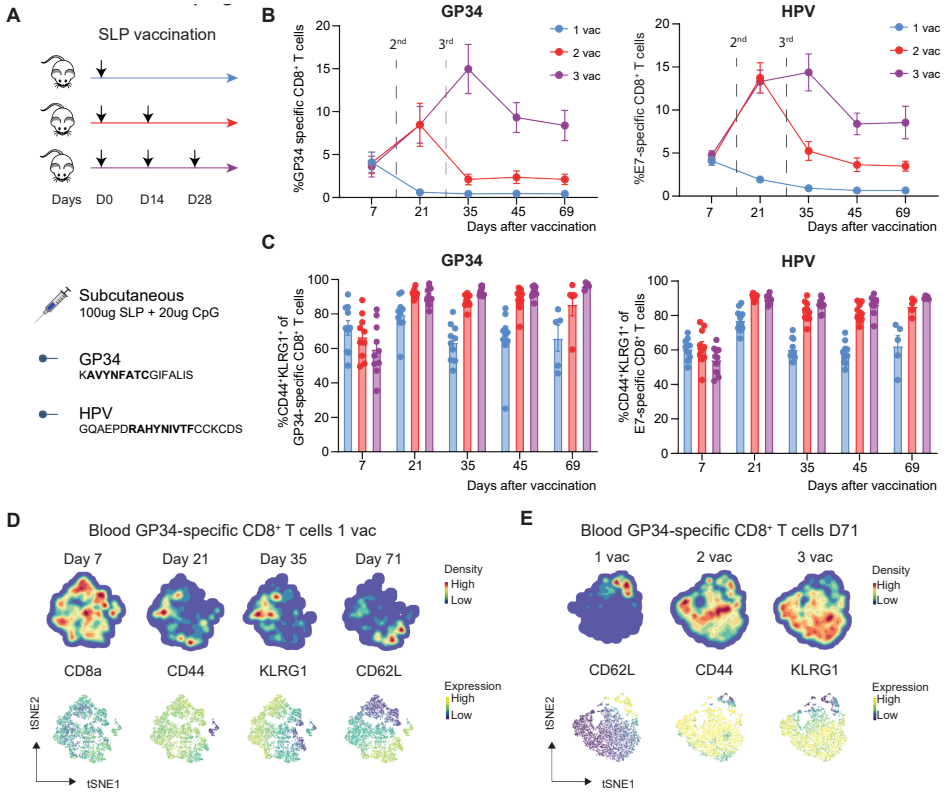

Figure 1. Prime-boost vaccination impacts the heterogeneity of circulating CD8⁺ T cells. A) Vaccination schedule for mice vaccinated with SLP vaccines in a prime-boost regimen with 2 week intervals. SLPs contain the dominant class I GP34 (LCMV) or E7 (HPV) epitope (epitope sequences are indicated in bold). B) Vaccine-specific CD8⁺ T cell kinetics in blood at indicated days after vaccination. Data +/- SEM are shown. C) Phenotype of GP34-specific or E7-specific CD8⁺ T cells in blood. Data +/- SEM are shown. D) Cytosplore tSNE analysis of GP34-specific CD8⁺ T cells at indicated time points after 1 vaccination. CD3, CD8a, CD62L, CD44, KLRG1 and GP34 tetramer were used for the analysis. The color of the cells indicates ArcSinh5-transformed expression values for a given marker analyzed. E) Cytosplore tSNE analysis of GP34-specific CD8⁺ T cells at day 71 after 1, 2 and 3 vaccinations. CD3, CD8a, CD62L, CD44, KLRG1 and GP34 tetramer were used for the analysis. See also Figure S1A.

Prime-boost vaccination increases protective antigen-specific memory T cells

To corroborate the differential impact of booster immunizations, the abundance of circulating and tissue-resident memory CD8⁺ T cells in blood, spleen and liver, was analyzed. Each vaccination with GP34 SLP, increased the percentage of antigen-specific CD8⁺ T cells in the blood circulation as well as in the spleen and liver (**Figure 2A and 2B**). In the liver, the increase of antigen-specific CD8⁺ T cells reached ~7% of total CD8⁺ T cells after 3 vaccinations, and of these antigen-specific CD8⁺ T cells, 40% expressed the tissue-resident marker CD69 (**Figure 2C**). A similar effect on the increment of antigen-specific CD8⁺ T cells upon boosting, was also observed after sequential E7 SLP vaccinations (**Figure 2D, 2E, 2F**).

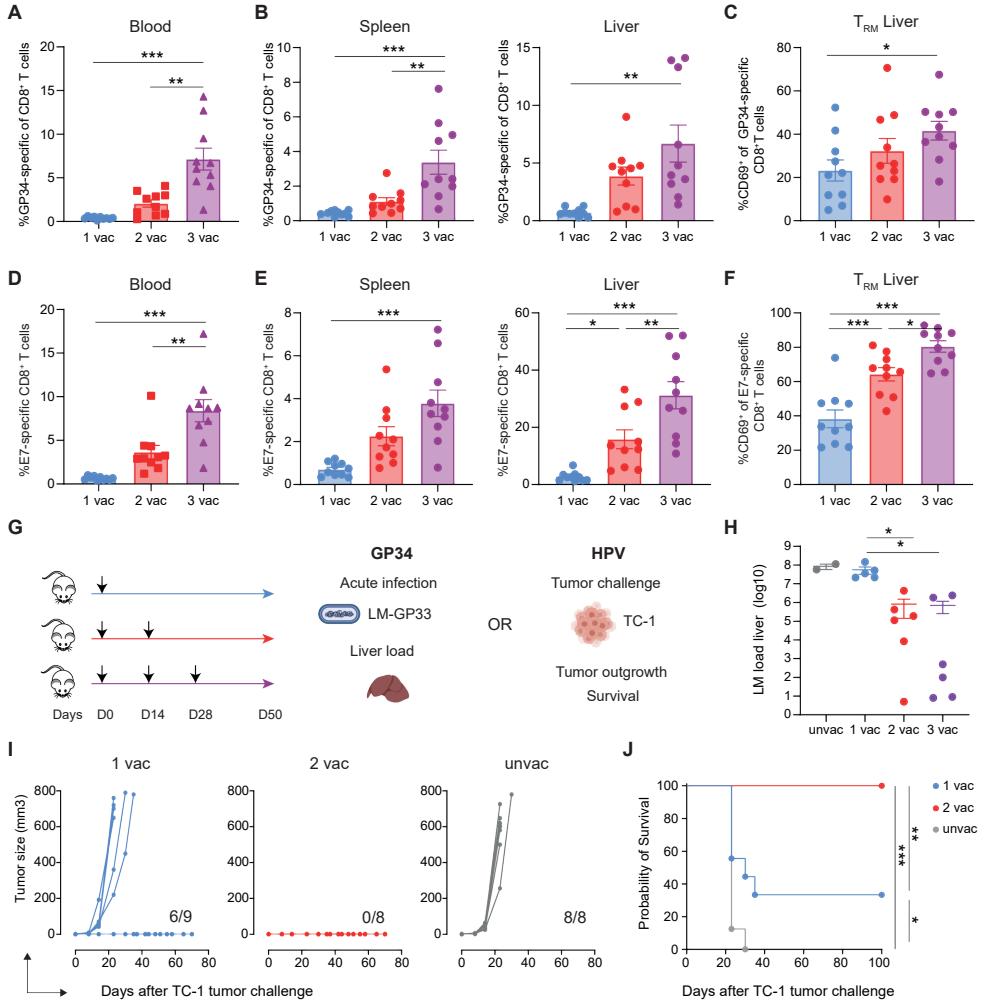

Figure 2. Prime-boost vaccination increases protective antigen-specific memory T cells. A) GP34-specific CD8⁺ T cell response in blood day 35 upon GP34 SLP vaccination. Data +/- SEM are shown (n=10 per group). B) GP34-specific CD8⁺ T cell response in spleen and liver day 50 upon GP34 SLP vaccinatinon. Data +/- SEM are shown (n=10 per group). C) GP34-specific CD8⁺ T_{RM} cell response in liver day 50 upon GP34 SLP vaccinatinon. Data +/- SEM are shown. D) E7-specific CD8⁺ T cell response in blood day 35 upon E7 SLP vaccinatinon. Data +/- SEM are shown (n=10 per group). E) E7-specific CD8⁺ T cell response in spleen and liver day 50 upon E7 SLP vaccinatinon. Data +/- SEM are shown (n=10 per group). F) E7-specific CD8⁺ T_{RM} cell response in liver day 50 upon E7 SLP vaccination. Data +/- SEM are shown. G-J) Experimental setup of bacterial and tumor challenge. At day 50 after the first GP34 vaccination mice received LM-GP33 challenge i.v. retro-orbitally. The bacterial load in liver was assessed 3 days after bacterial challenge (H). At day 50 after the first E7 SLP vaccination mice received a TC-1 tumor challenge s.c. in the flank. Upon tumor challenge, tumor outgrowth (I) and survival (J) were assessed. One-way ANOVA and log-rank (Mantel-Cox) survival test were used for statistical analysis. *P<0.05, **P<0.01. ANOVA, analysis of variance.

To determine whether this increase in antigen-specific memory CD8⁺ T cells correlates to increased protection, mice where challenged with *Listeria Monocytogenes* (LM), a gram-positive bacterium that replicates within the host cell cytosol (29, 30), containing the GP34 epitope (LM-GP34), or received a TC-1 tumor challenge upon GP34 and E7 SLP vaccination, respectively (**Figure 2G**). Booster vaccination with GP34 SLP increased protection against LM-GP33 (**Figure 2H**), but this protection was not further improved by a second boost. Similar results were obtained when E7 SLP vaccinated mice challenged with TC-1 tumor cells. Here, a single E7 SLP vaccination did partially protect mice from tumor outgrowth whereas an additional booster vaccination fully protected mice (**Figure 2I, 2J**). Thus, SLP booster vaccination increases the magnitude of antigen-specific memory CD8⁺ T cells leading to enhanced protection against infection and malignant disease.

Prime-boost antigen triggering impacts phenotype of antigen-specific CD8⁺ T cells organ-wide

To study in depth the phenotype of the antigen-specific CD8⁺ T cells induced upon sequential SLP vaccinations, we performed single-cell high dimensional mass cytometry (**Figure 3A**). Our panel includes 39 cellular markers that allows an in depth identification of T cell signatures as previously described (**Table S1**) (21). For the detection of PE- and APC-labelled MHC class I tetramer-binding T cells, anti-PE and anti-APC antibodies coupled to lanthanides were added to the panel. Upon selection of live single cells, positive for CD45, files were compensated using Catalyst (22), after which tetramer-specific CD8⁺ T cells were selected in FlowJo (**Figure S1B and S1C**). To interrogate whether the phenotype of antigen-specific CD8⁺ T cells is influenced by sequential vaccinations and the tissue environment, we performed a system-wide analysis of antigen-specific CD8⁺ T cell subsets in all tissues examined after multiple vaccinations. Analysis of antigen-specific CD8⁺ T cells was performed using Cytosplore (23) and subsequent dual tSNE and Jensen-Shannon (JS) divergence analysis.

First, we visualized the similarity between GP34-specific CD8⁺ T cells that were present in spleen, liver, lungs, and bone marrow upon 1, 2 or 3 vaccinations in one tSNE analysis (**Figure 3B-D**). This analysis shows that distinct patterns exist across sequential vaccinations (**Figure 3B**). Especially the first boost has a profound impact on the phenotype of these vaccine-induced CD8⁺ T cells whereas the second boost further shaped the phenotype of these cells, albeit less evident. Visualization of the tSNE distribution across different tissues revealed

that antigen-specific CD8+ T cells cluster together depending on their location (**Figure 3C**). Here, liver and lung tissue have a similar phenotype, as well as hematopoietic tissues spleen and bone marrow. The cell distribution in this analysis is based on expression of all markers in our panel and the abundance of the various clusters. Using this approach clusters of CD8+ T_{EM} and CD8+ T_{RM} cells were identified, by their expression of CD62L, KLRG1, CD69, CX3CR1 (**Figure 3D**).

Subsequently, we performed a dual tSNE analysis on all 60 samples of GP34-specific CD8+ T cells (three vaccinations, four tissues, n = 5) based on the abundance of 63 GP34-specific CD8+ T cell clusters generated by Cytosplore. We visualized the segregation of the samples, based on vaccination-associated patterns or tissue-specific patterns. The distribution of samples showed clusters of BM and spleen or lung and liver but also clusters of vaccinations were evident. In addition to the sample distribution, visualization of the tSNE map values of the GP34-specific CD8+ T cell clusters corroborated the tissue- and vaccination-associated patterns (**Figure 3E and 3F**). The GP34-specific CD8+ T cell clusters contributing to the 2nd and 3rd vaccination-specific phenotypes had considerable overlap. Subsequently, the similarity between the tSNE plots of memory CD8+ T cell clusters in multiple vaccinations and in different tissues was determined by performing a Jensen-Shannon (JS) divergence analysis (**Figure 3G**). A low JS distance was found when comparing antigen-specific CD8+ T cells induced upon 2 and 3 vaccinations, indicating high similarities between cells induced upon these vaccinations, whereas a higher JS distance was found when comparing 1 to 2 vaccinations or 1 to 3 vaccinations. In contrast, for all tissues high JS distance was obtained, indicating that tissues induce clear dissimilar tissue-specific CD8+ T cell states. Thus, upon sequential SLP vaccinations, antigen-specific CD8+ T cells have their unique phenotype in multiple organs and especially after the first boost the phenotype is different from the initial vaccination.

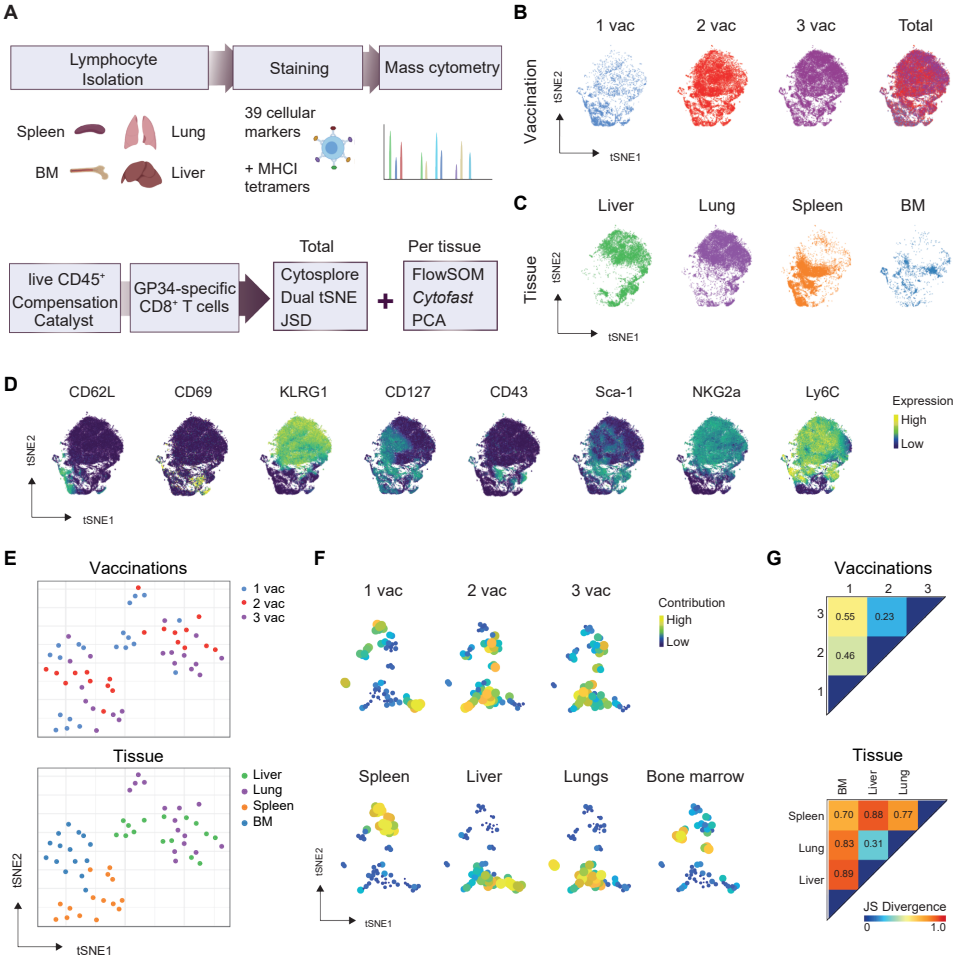

Figure 3. Prime-boost antigen triggering impacts phenotype of antigen-specific CD8⁺ T cells organ-wide. A) Experimental setup and data analysis graphic. Mice were vaccinated s.c. tailbase with GP34 SLP (100ug) + CpG (20ug) with 2 week intervals. At day 72 after the first vaccination, lymphocytes were isolated from spleen, liver, lung and bone-marrow. Spleen and bone-marrow were T cell enriched, liver and lung lymphocytes were isolated using a Percoll gradient. Lymphocytes were stained for mass cytometry analysis. For data analysis, CD45 live cells were manually gated in FlowJo, after which samples were compensated using Catalyst. After gating GP34-specific CD8⁺ T cells in FlowJo, data was analyzed using Cytosplore and subsequent dual tSNE and JSD analysis or data was analyzed per tissue using FlowSOM and Cytofast, as well as PCA analysis. Figure created with BioRender. B, C) tSNE embedding of GP34-specific CD8⁺ T cells isolated from vaccinated mice and multiple organs in one analysis. Cells are color coded per vaccination (B) of type of tissue (C). D) Expression intensity of the cell-surface markers on the GP34-specific CD8⁺ T cells. The color of the cells indicates ArcSinh5-transformed expression values for a given marker analyzed. E, F) dual tSNE analysis of GP34-specific CD8⁺ T cells from multiple organs (liver, lung, spleen, bone-marrow) of mice (n = 5 per vaccination group) that received 1, 2 or 3 vaccinations. E) tSNE maps showing the 60 samples, color coded per vaccination (upper) or per tissue (below). Samples with similar composition across clusters end up close together in the map. F) tSNE maps showing the 63 GP34-specific CD8⁺ T cell clusters per vaccination (upper row) or tissue (lower row). Clusters with similar composition profiles across samples end up close together in the map. The varying dot size and color in this cluster tSNE map shows the average cluster normalized frequencies per vaccination/tissue group. G) Pairwise Jensen-Shannon Divergence plots of the tSNE map obtained from all samples of GP34-specific CD8⁺ T cells grouped by vaccinations (upper) and tissue (lower). JSD, Jensen-Shannon Divergence. PCA, Principal Component Analysis. See also Figure S1B.

Heterogeneity of CD8+ T_{EM} and T_{RM} cells upon vaccination

To gain further insight into the phenotypic heterogeneity within the antigen-specific CD8+ T cell pools in the different organs, we performed Principal Component Analysis (PCA) per tissue based on the cluster frequencies of the GP34-specific memory CD8+ T cells. The clusters present in liver, spleen, lung and bone-marrow were clearly distinct between one vaccination and booster vaccinations, indicating booster-specific clustering of the GP34-specific CD8+ T cell populations (**Figure 4A**).

To gain further insight into the antigen-specific CD8+ T cell phenotypes in the different organs, we analyzed the phenotype of these cells per tissue using FlowSOM and Cytofast (28) and confirmed and visualized the data using Cytosplore. Using FlowSOM, 14 clusters were generated per analysis, of which we show here the clusters abundant >5% of total antigen-specific CD8+ T cells that show a difference between the vaccination groups. In the liver, 2 subsets of GP34-specific CD8+ T cells increased upon boosting (**Figure 4B**). Specifically, one subset expressing KLRG1 and CX3CR1, Ly6C and NKG2A was increased upon the first booster vaccination to almost 70% of total antigen-specific CD8+ T cells in the liver. On the contrary, a subset expressing CD127 but lacking other activation markers was decreased upon boosting. Also, one GP34-specific CD8+ T_{RM} cluster was slightly increased upon boosting. We confirmed these data and visualized the cellular distribution and marker expression by one tSNE analysis on the same GP34-specific CD8+ T cells from liver using Cytosplore (**Figure 4C**). In the spleen, two GP34-specific CD8+ T_{CM} subsets decreased upon boosting and one CD8+ T_{EM} subset increased with a phenotype similar to the liver CD8+ T_{EM} cells (**Figure 4D and Figure S2A**). Here, for both liver and spleen, using Cytofast as well as Cytosplore analysis, we confirmed the change in phenotype especially upon the first vaccine boosting. However, using this approach we are not able to study the heterogeneity of CD8+ T_{RM} cells because of their relative low abundance. When we zoom in on the CD69+ CD8+ T_{RM} cells using Cytosplore and analyse these using Cytofast, we can further identify and visualize various antigen-specific CD8+ T_{RM} cell clusters (**Figure 4E**). Here, contrary to the first boost effect on the CD8+ T_{EM} cells, mainly the second booster vaccination has an impact on the phenotype of CD8+ T_{RM} cells, increasing antigen-specific CD8+ T_{RM} cells that express CD11c, CD49a and Sca-1. Next to the antigen-specific CD8+ T cells in spleen and liver, we analyzed the heterogeneity of antigen-specific CD8+ T cells in lung and bone marrow (**Figure S2B-E**). Also in both lungs and bone marrow, the phenotype was mainly affected by the first boost. We confirmed these antigen-specific CD8+ T_{RM} and T_{EM} phenotypes using flow cytometry (**Figure S3**). Thus, booster vaccination impacts the heterogeneity of antigen-specific CD8+ T_{EM} and T_{RM} cells organ-wide.

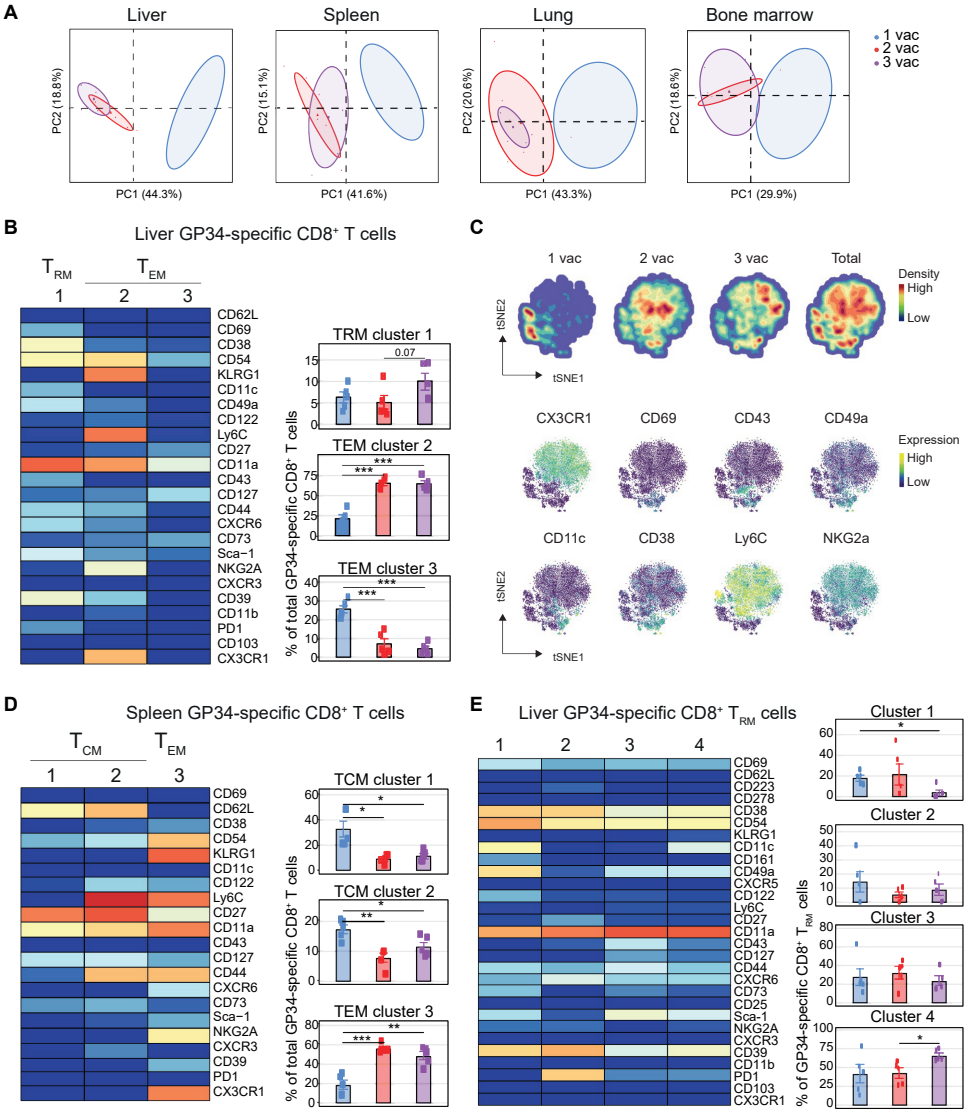

Figure 4. Heterogeneity of CD8⁺ T_{EM} and T_{RM} cells upon vaccination. A) Principal Component Analysis of GP34-specific CD8⁺ T cells per tissue upon multiple vaccinations. B) Mass cytometry data of GP34-specific CD8⁺ T cells in the liver of mice that received multiple vaccinations. Level of ArcSinh5transformed expression marker is displayed by a rainbow scale. Average and SEM in percentage of each CD8⁺ T cell cluster among the GP34-specific CD8⁺ T-cell population of one vaccination (blue bars), two vaccinations (red bars) and three vaccinations (purple bars). C) tSNE embeddings of liver GP34-specific CD8⁺ T cells isolated from vaccinated mice. Distribution of GP34-specific CD8⁺ T cells per vaccination in one tSNE analysis. Expression intensity of the cell-surface markers on the GP34-specific CD8⁺ T cells. The color of the cells indicates ArcSinh5-transformed expression values for a given marker analyzed. D) Mass cytometry data of GP34-specific CD8⁺ T cells in the spleen of mice that received multiple vaccinations. E) Mass cytometry data of GP34-specific CD8⁺ T_{RM} cells in the liver of mice that received multiple vaccinations. See also Figure S2 and S3.

CD69+ CD8+ T cells induced in liver upon vaccination and infection express Hobit

To determine specifically the impact of antigen-triggering by prime-boost-boost vaccination on antigen-specific CD8+ T_{RM} cells, we adoptively transferred Hobit reporter OT-I cells and studied subsequent CD8+ T cell responses upon vaccination and infection. These Hobit reporter cells are TCR transgenic OT-I cells, recognizing the OVA-derived peptide SIINFEKL (10), and contain tdTomato in the Hobit locus. This enables us to study antigen-specific T cell responses after OVA SLP vaccination as well as after infection with pathogens that contain the OVA epitope. First, we confirmed that OVA SLP prime-boost-boost vaccination, by subcutaneously administration in a 2 week interval together with TLR9 adjuvant CpG, induced antigen-specific CD8+ T cell responses comparable to the other SLPs (**Figure 5A**). Upon OVA SLP vaccination, sequential SLP vaccinations increased the percentage of OVA-specific CD8+ T cells in the circulation as well as the spleen and liver day 50 after the first vaccination (**Figure 5B and 5C**). In addition, OVA SLP vaccination induced antigen-specific CD8+ T_{RM} cells in multiple tissues, similar to GP34 and E7 SLP vaccination (**Figure S4**). Upon sequential vaccination, an increase of antigen-specific CD8+ T cells was seen in liver, where upon 3 vaccinations these antigen-specific CD8+ T cells reached on average 8% of total CD8+ T cells. To determine whether the CD69+ antigen-specific CD8+ T cells are truly tissue-resident, we performed an adoptive transfer of Hobit OT-I reporter cells (**Figure 5D**). One day after adoptive transfer of Hobit reporter cells, mice received the viral MCMV-OVA infection, bacterial LM-OVA infection or 3 times vaccination with OVA SLP with two weeks interval. Using flow cytometry, we tracked the presence of these cells in the circulation, by their expression of CD45.1 (**Figure 5E**). As expected upon acute infection, challenge with *Listeria Monocytogenes*-OVA resulted in a peak of CD45.1+ cells at day 8 after infection followed by contraction. However, SLP boosting increased the CD45.1+ cells over time, with the peak after the 3rd boost. Upon infection with MCMV-OVA, CD45.1+ cells were maintained. In the circulation, the adoptively transferred cells did not express Hobit since, confirming the lacking of residency (**Figure 5F**). In the liver, the transferred Hobit reporter cells can be found 50 days after adoptive transfer upon SLP boost as well as acute and persistent infection. SLP prime-boost-boost vaccination elicited most CD45.1+ cells in liver, more than 60% of total CD8+ T cells. Thus, strong antigen-triggering by SLP vaccination induced potent expansion of these adoptively transferred cells. Moreover, a large subset of these cells in liver expressed CD69 (**Figure 5G**). In all experimental settings, the CD69+ CD45.1+ T cells from liver express Hobit, confirming tissue-residence (**Figure 5H**).

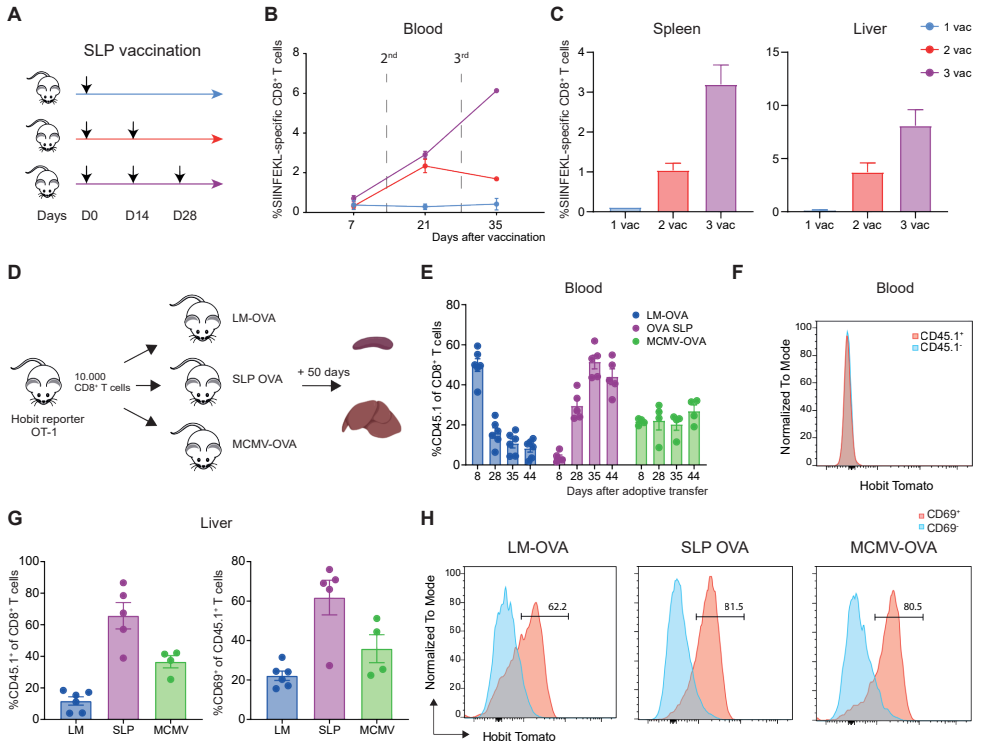

Figure 5. CD69⁺ CD8⁺ T cells induced in liver upon vaccination and infection express Hobit. A) Mice were vaccinated s.c. tailbase with OVA SLP (100ug) + CpG (20ug) in a prime-boost regimen with 2 week intervals. B) OVA-specific CD8⁺ T cell kinetics in blood at indicated days after vaccination. Data +/- SEM are shown. C) OVA-specific CD8⁺ T cell response in spleen and liver day 50 after the first OVA SLP vaccinatinon. Data +/- SEM are shown (n=2 per group). D) Schematic overview of experimental setup. 10.000 Hobit OT-I CD8⁺ T cells were adoptively transferred into C57BL/6 mice. The day after, mice received the first SLP OVA vaccination, which continued in a prime-boost-boost setting, or $1x10^4$ CFU LM-OVA retro-orbitally i.v. or $1x10^4$ IU MCMV-IE2 OVA i.p. infection and after 50 days spleen and liver CD8⁺ T cells were isolated and analyzed by flow cytometry. Figure created with Biorender. E) Percentage of CD45.1⁺ T cells in blood at indicated time points after vaccination. F) Expression of Hobit in CD45.1⁺ and CD45.1⁻ T cells in blood day 44 after MCMV-IE2 OVA infection. G) Percentage of CD45.1⁺ and CD69⁺ T cells in liver day 50 after vaccination or infection. H) Expression of Hobit in CD69⁺ and CD69⁻ populations from CD45.1⁺ cells in liver 50 days after SLP vaccination or LM-OVA or MCMV-OVA infection. See also Figure S4.

Ex-T_{RM} cells induced in circulation and liver upon booster vaccination

To investigate whether ex-T_{RM} cells are generated upon antigen-triggering, we adoptively transferred Hobit lineage tracer (LT) CD8⁺ T cells into naïve CD45.2 wild-type mice that received subsequent SLP vaccinations or MCMV infection. We used these reporter cells to fate map T_{RM} cell progeny by exploiting T_{RM} transcription factor Hobit (10). Here, Hobit reporter OT-I mice were crossed with ROSA26-eYFP mice, resulting in constitutive expression of YFP in Hobit-expressing T cells. The day after adoptive transfer, mice received OVA SLP vaccination

in a prime-boost-boost setting or MCMV-OVA infection to investigate the antigen-specific expansion of transferred cells (**Figure 6A**). We studied the phenotype of memory CD8+ T cells and the formation of CD8+ ex-T_{RM} cells in spleen and liver day 50 after adoptive transfer. Here we used MCMV as a model of low level antigen-triggering, compared to prime-boost-boost SLP vaccination that induces strong antigen-triggering. MCMV induces CD8+ T cells against various epitopes, and is well known to induce memory inflation, a phenomenon where T cell populations specific for certain epitopes do not contract but instead are maintained and/or accumulate at high frequencies (31). Here we used MCMV expressing OVA under the IE2 or M45 promotor, inducing inflationary and non-inflationary OVA responses respectively (32).

Upon adoptive transfer and subsequent SLP vaccination, CD8+ ex-T_{RM} cells are induced in the circulation after booster vaccination, and the presence increases substantially upon a sequential second boost (**Figure 6B**). Remarkably, one week after a third SLP vaccination, almost 4% of total CD8+ T cells in the circulation are ex-T_{RM} cells, even though we only transferred 10.000 CD8+ Hobit LT T cells. Upon MCMV infection, CD8+ ex-T_{RM} cells are present in the circulation even though at much lower frequency. Moreover, the presence of ex-T_{RM} cells in circulation slightly decreased over time upon infection with MCMV-M45 OVA compared to MCMV-IE2 OVA (**Figure 6B**). Day 50 after adoptive transfer we analyzed the memory CD8+ T cell composition in the spleen and liver. In the liver, an increase of CD8+ T_{RM} cells and CD8+ ex-T_{RM} cells was found upon first and second SLP boosting (**Figure 6C**). Of these CD8+ T_{RM} cells, expressing both YFP and tomato, all cells express CD69 in liver (**Figure 6D**). No difference in CD8+ T_{RM} cell or CD8+ ex-T_{RM} cell formation was found upon MCMV-IE2 OVA or MCMV-M45-OVA infection (**Figure 6E**). CD8+ ex-T_{RM} cells were increased in both liver and spleen, however the highest frequency was found in spleen upon the second boost. In line with previous findings, we found that CD8+ ex-T_{RM} in spleen and liver mainly acquire an T_{EM} phenotype (**Figure 6F-H**). Thus, ex-T_{RM} cells induced upon sequential SLP vaccination are present in the circulation, spleen and liver.

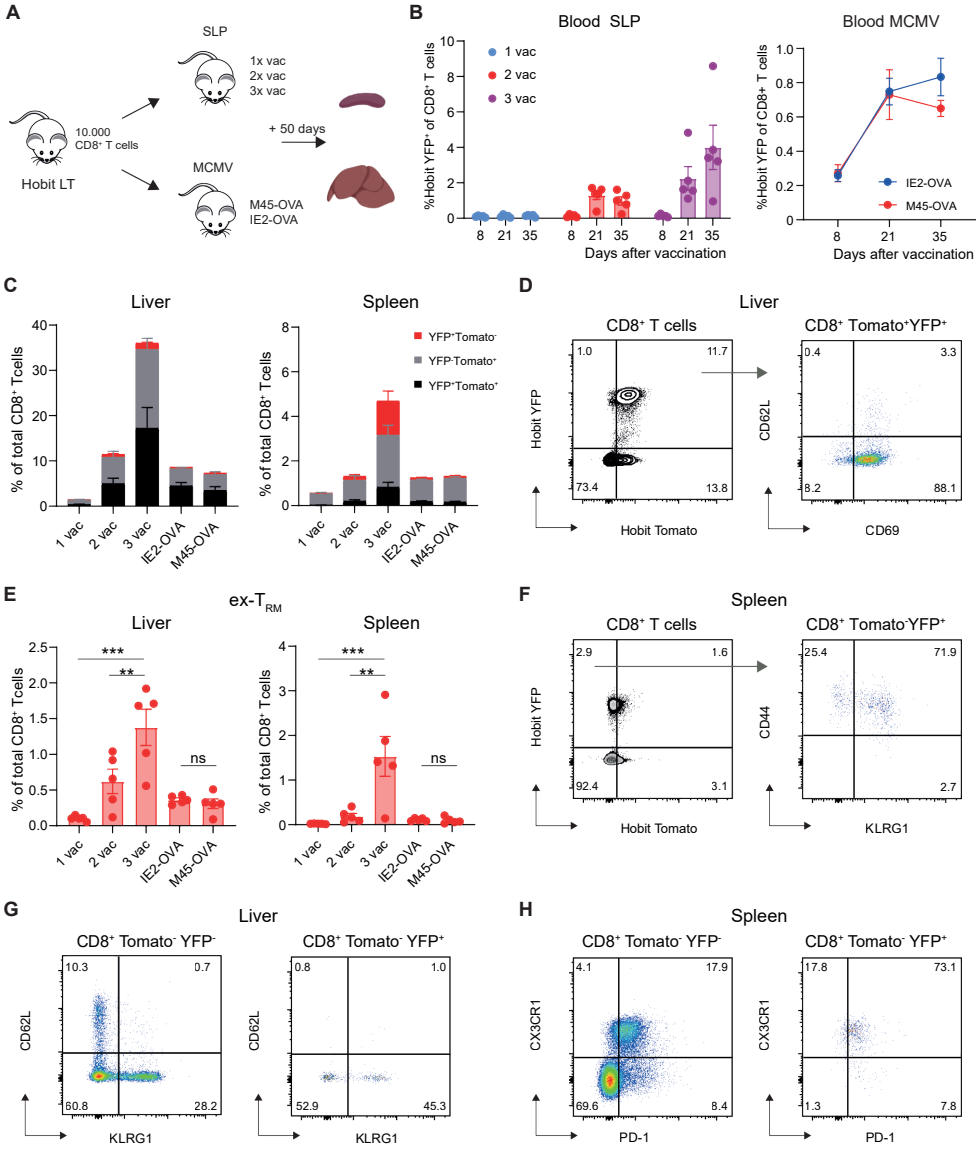

Figure 6. Prime-boost vaccination increases antigen-specific CD8⁺ ex-T_{RM} cells. A) Schematic overview of experimental setup. 10.000 Hobit LT CD8⁺ T cells were adoptively transferred into C57BL/6 mice. The day after, mice received the first GP34 SLP vaccination, which continued in a prime-boost-boost setting, 1x10⁴ IU MCMV-IE2 OVA i.p. or 1x10⁴ IU MCMV-M45 OVA i.p. infection and after 50 days spleen and liver were analyzed by flow cytometry. B) Percentage of Hobit YFP⁺ T cells of total CD8⁺ T cells in blood. C) Phenotype of total CD8⁺ T cells in liver and spleen. D) Flow cytometry plots showing phenotype of liver YFP⁺ Tomato⁺ CD8⁺ T cells. E) Percentage of ex-T_{RM} of total CD8⁺ T cells in liver and spleen. F) Phenotype of ex-T_{RM} CD8⁺ T cells in spleen. G, H) Phenotype of Tomato⁻YFP⁻ CD8⁺ T cells and ex-T_{RM} CD8⁺ T cells in liver (G) and spleen (H). One-way ANOVA was used for statistical analysis. *P<0.05, **P<0.01. ANOVA, analysis of variance.

Discussion

In this study, we show that SLP prime-boost-boost antigen triggering impacts the differentiation of circulating CD8+ T cells and increases the amount of antigen-specific CD8+ T cells in multiple organs, leading to increased protection against bacterial infection and tumor challenge. Moreover, prime-boost vaccination induced both circulating and tissue-resident memory CD8+ T cell populations, with a heterogeneous phenotype in multiple organs. In addition, prime-boost-boost vaccination increased antigen-specific CD8+ ex-T_{RM} cells in the circulation as well as liver and spleen.

Previous studies showed an increase in memory CD8+ T cell responses and protective immunity by sequential immunizations. Jiang et al. showed that T_{RM} cells generated by localized skin infection reside not only in the site of infection, but also populate the entire skin surface (7). Moreover, repeated re-infections led to progressive accumulation of protective T_{RM} cells in non-involved skin. In line with these findings, Davies et al. showed that repeated boosting enhanced T_{RM} development and dissemination throughout the skin, providing enhanced immunity (33). Recently, a synthetic conjugate vaccine has been developed to induce protective liver T_{RM} cells (34). This glycolipid-peptide vaccine induced liver-resident memory CD8+ T cells protective against rodent malaria. A single dose of this synthetic conjugate vaccine induced substantial numbers of intrahepatic malaria-specific CD8+ T_{RM} cells that could be further increased in number upon vaccine boosting.

In this study, we aimed to understand the impact of repeated boosting on circulating as well as tissue-resident memory T cell differentiation in multiple tissues. We found that the boosting impacts the phenotype and abundance of memory T cells organ-wide. For both GP34, E7 and OVA SLP, boosting increased antigen-specific CD8+ T cell in the circulation as well as the spleen and liver. Upon the first boost, mice were protected against bacterial and tumor challenge. In line with these findings, antigen-specific CD8+ T_{EM} phenotypes were mainly affected by the first boost and an additional second boosting only had a minor impact on the antigen-specific CD8+ T cell phenotypes. However, mainly the second boost impacted the phenotype of CD8+ T_{RM} cells. In addition, ex-T_{RM} cells were induced in liver and increase in the spleen especially after the second boost. Further investigation is needed to delineate the role of ex-T_{RM} cells in protection.

Here, we confirmed the findings of repeated boosting with three different SLPs. Vaccination with E7 SLP generated much higher frequencies of antigen-specific $CD8^+$ T cells compared to GP34. Moreover, remarkably 80-90% of these antigen-specific $CD8^+$ T cells had a tissue-resident phenotype in the liver. On the contrary, vaccination with GP34 OVA peptide generated weaker $CD8^+$ T cell responses, even though booster effects were similar. Thus, both GP34, OVA and E7 peptide booster vaccinations increased the antigen-specific memory $CD8^+$ T cell response but the phenotype of these cells differed between different peptides. The difference in $CD8^+$ T cell response might be explained by the length of the peptide or the inclusion of a CD4 T cell help epitope, which needs further investigation. However, our previous studies showed that protective immune responses induced by SLP vaccination is mainly attributable to $CD8^+$ T cells, not $CD4^+$ T cell or antibody responses (35).

In this study we used SLP vaccines in combination with TLR9 ligand CpG as adjuvant. Previously it was found that DC-activating adjuvant CpG together with prime-boost long peptide vaccinations increases efficacy and leads to eradications of established tumors (36). CpG increases frequencies of effector-memory cells after vaccination in nontumor settings, which correlate with a superior effect of these vaccines on inhibiting tumor outgrowth when used as therapeutic vaccines (37). SLP vaccines are interesting vaccine candidates because they can be conjugated to various molecules that enhance strong T cell responses and thereby improve their efficacy. SLPs can be conjugated to TLR ligands, to strongly enhance the induction of antitumor immunity (38). Also OX40 ligation during booster vaccination with a mixture SLPs leads to the induction of strong and polyfunctional $CD8^+$ T cell responses (39). Additionally, SLP vaccination can be combined with chemotherapeutics such as cisplatin to improve clinical outcomes (40). For further studies it would be interesting to delineate the heterogeneity of antigen-specific circulating as well as tissue-resident $CD8^+$ T cell populations upon SLP conjugation or combination therapies.

We have previously reported that the phenotypic heterogeneity of $CD8^+$ T_{EM} and $CD8^+$ T_{RM} cells is influenced by both the pathogen environment as well as tissue-specific cues (21). For various viral and bacterial infections, the phenotype of both antigen-specific as well as total $CD8^+$ T cells differs amongst different hematopoietic and non-hematopoietic tissues. This is in line with our findings with peptide vaccinations, where antigen-specific $CD8^+$ T cells show tissue-specific phenotypes. A better understanding of the development and heterogeneity of

these antigen-specific CD8+ T_{RM} cells in different organs upon booster vaccination may help improve vaccination and immunotherapeutic strategies in infectious or malignant disease (41).

To summarize, we studied in depth the effects of vaccine boosting on the antigen-specific circulating and tissue-resident CD8+ T cell responses organ-wide. Subset of antigen-specific memory CD8+ T cells, including T_{EM}, T_{RM} and ex-T_{RM} cells, increased by booster vaccination in multiple tissues. Understanding the induction of long-lasting antigen-specific memory CD8+ T cell responses is critical for the design of vaccines against infectious or malignant diseases.

Author contributions

Conceptualization: E.T.I.v.d.G. and R.A.; Methodology: E.T.I.v.d.G., F.K., K.P.J.M.G. and R.A.; Analysis and Visualization: E.T.I.v.d.G., G.B., T.A.; Investigation: E.T.I.v.d.G., G.B., E.B.N., F.M.B, T.H.W..; Writing—Original draft: E.T.I.v.d.G. and R.A.; Writing—Review & Editing: E.T.I.v.d.G., F.K., and R.A.; Supervision: R.A.; Funding Acquisition: E.T.I.v.d.G. and R. A.

Acknowledgements

We would like to thank the LUMC Animal Core Facility and the LUMC Flow Cytometry Core Facility for their support. We thank Kees Franken for generating MHC class I tetramers and Dena Brasem and Suzanne van Duikeren for technical assistance with experiments.

Funding

This work was supported by a BWplus grant from the LUMC and the graduate program of the Dutch Research Council (awarded to EvdG) and a Dutch Cancer Society grant (KWF UL2015-7817 awarded to RA).

References

1. Seder RA, Darrah PA, Roederer M. T-cell quality in memory and protection: implications for vaccine design. Nature Reviews Immunology. 2008;8(4):247-58.
2. Panagioti E, Klenerman P, Lee LN, van der Burg SH, Arens R. Features of Effective T Cell-Inducing Vaccines against Chronic Viral Infections. Frontiers in immunology. 2018;9:276-.
3. Logunov DY, Dolzhikova IV, Shcheblyakov DV, Tukhvatulin AI, Zubkova OV, Dzharullaeva AS, et al. Safety and efficacy of an rAd26 and rAd5 vector-based heterologous prime-boost COVID-19 vaccine: an interim analysis of a randomised controlled phase 3 trial in Russia. Lancet. 2021.
4. Swadling L, Capone S, Antrobus RD, Brown A, Richardson R, Newell EW, et al. A human vaccine strategy based on chimpanzee adenoviral and MVA vectors that primes, boosts, and sustains functional HCV-specific T cell memory. Sci Transl Med. 2014;6(261):261ra153.
5. Pollard AJ, Bijker EM. A guide to vaccinology: from basic principles to new developments. Nature Reviews Immunology. 2021;21(2):83-100.
6. Barrett JR, Belij-Rammerstorfer S, Dold C, Ewer KJ, Folegatti PM, Gilbride C, et al. Phase 1/2 trial of SARS-CoV-2 vaccine ChAdOx1 nCoV-19 with a booster dose induces multifunctional antibody responses. Nat Med. 2020.
7. Jiang X, Clark RA, Liu L, Wagers AJ, Fuhlbrigge RC, Kupper TS. Skin infection generates non-migratory memory CD8+ T(RM) cells providing global skin immunity. Nature. 2012;483(7388):227-31.
8. Mackay LK, Braun A, Macleod BL, Collins N, Tebartz C, Bedoui S, et al. Cutting edge: CD69 interference with sphingosine-1-phosphate receptor function regulates peripheral T cell retention. J Immunol. 2015;194(5):2059-63.
9. van der Gracht ET, Schoonderwoerd MJ, van Duikeren S, Yilmaz AN, Behr FM, Colston JM, et al. Adenoviral vaccines promote protective tissue-resident memory T cell populations against cancer. Journal for ImmunoTherapy of Cancer. 2020;8(2):e001133.
10. Behr FM, Parga-Vidal L, Kragten NAM, van Dam TJP, Wesselink TH, Sheridan BS, et al. Tissue-resident memory CD8(+) T cells shape local and systemic secondary T cell responses. Nat Immunol. 2020;21(9):1070-81.
11. Fonseca R, Beura LK, Quarnstrom CF, Ghoneim HE, Fan Y, Zebley CC, et al. Developmental plasticity allows outside-in immune responses by resident memory T cells. Nat Immunol. 2020;21(4):412-21.
12. Stolley JM, Johnston TS, Soerens AG, Beura LK, Rosato PC, Joag V, et al. Retrograde migration supplies resident memory T cells to lung-draining LN after influenza infection. J Exp Med. 2020;217(8).
13. Melief CJM, van der Burg SH. Immunotherapy of established (pre)malignant disease by synthetic long peptide vaccines. Nature Reviews Cancer. 2008;8:351.
14. Melief CJM, Welters MJP, Vergote I, Kroep JR, Kenter GG, Ottevanger PB, et al. Strong vaccine responses during chemotherapy are associated with prolonged cancer survival. Sci Transl Med. 2020;12(535).
15. Welten SP, Redeker A, Franken KL, Oduro JD, Ossendorp F, Cicin-Sain L, et al. The viral context instructs the redundancy of costimulatory pathways in driving CD8(+) T cell expansion. Elife. 2015;4.
16. Dekhtiarenko I, Jarvis MA, Ruzsics Z, Čičin-Šain L. The Context of Gene Expression Defines the Immunodominance Hierarchy of Cytomegalovirus Antigens. J Immunol. 2013;190(7):3399-409.
17. Foulds KE, Zenewicz LA, Shedlock DJ, Jiang J, Troy AE, Shen H. Cutting Edge: CD4 and CD8 T Cells Are Intrinsically Different in Their Proliferative Responses. The Journal of Immunology. 2002;168(4):1528-32.
18. Lin KY, Guarnieri FG, Staveley-O'Carroll KF, Levitsky HI, August JT, Pardoll DM, et al. Treatment of established tumors with a novel vaccine that enhances major histocompatibility class II presentation of tumor antigen. Cancer research. 1996;56(1):21-6.
19. Mei HE, Leipold MD, Maecker HT. Platinum-conjugated antibodies for application in mass cytometry. Cytometry A. 2016;89(3):292-300.
20. Spitzer MH, Carmi Y, Reticker-Flynn NE, Kwek SS, Madhireddy D, Martins MM, et al. Systemic Immunity Is Re-

quired for Effective Cancer Immunotherapy. Cell. 2017;168(3):487-502.e15.
21. van der Gracht ETI, Beyrend G, Abdelaal T, Pardieck IN, Wesselink TH, van Haften FJ, et al. Memory CD8+ T cell heterogeneity is primarily driven by pathogen-specific cues and additionally shaped by the tissue environment. iScience. 2021;24(1):101954.
22. Chevrier S, Crowell HL, Zanotelli VRT, Engler S, Robinson MD, Bodenmiller B. Compensation of Signal Spillover in Suspension and Imaging Mass Cytometry. Cell Systems. 2018;6(5):612-20.e5.
23. Höllt T, Pezzotti N, van Unen V, Koning F, Eisemann E, Lelieveldt B, et al. Cytosplore: Interactive Immune Cell Phenotyping for Large Single-Cell Datasets. Computer Graphics Forum. 2016;35(3):171-80.
24. Van Gassen S, Callebaut B, Van Helden MJ, Lambrecht BN, Demeester P, Dhaene T, et al. FlowSOM: Using self-organizing maps for visualization and interpretation of cytometry data. Cytometry A. 2015;87(7):636-45.
25. van Unen V, Höllt T, Pezzotti N, Li N, Reinders MJT, Eisemann E, et al. Visual analysis of mass cytometry data by hierarchical stochastic neighbour embedding reveals rare cell types. Nature Communications. 2017;8(1):1740.
26. Pezzotti N, Lelieveldt BPF, Van Der Maaten L, Hollt T, Eisemann E, Vilanova A. Approximated and User Steerable tSNE for Progressive Visual Analytics. IEEE Trans Vis Comput Graph. 2017;23(7):1739-52.
27. van Unen V, Li N, Molendijk I, Temurhan M, Hollt T, van der Meulen-de Jong AE, et al. Mass Cytometry of the Human Mucosal Immune System Identifies Tissue- and Disease-Associated Immune Subsets. Immunity. 2016;44(5):1227-39.
28. Beyrend G, Stam K, Hollt T, Ossendorp F, Arens R. Cytofast: A workflow for visual and quantitative analysis of flow and mass cytometry data to discover immune signatures and correlations. Comput Struct Biotechnol J. 2018;16:435-42.
29. Busch DH, Pilip IM, Vijh S, Pamer EG. Coordinate Regulation of Complex T Cell Populations Responding to Bacterial Infection. Immunity. 1998;8(3):353-62.
30. Pope C, Kim SK, Marzo A, Masopust D, Williams K, Jiang J, et al. Organ-specific regulation of the CD8 T cell response to Listeria monocytogenes infection. J Immunol. 2001;166(5):3402-9.
31. O'Hara GA, Welten SP, Klenerman P, Arens R. Memory T cell inflation: understanding cause and effect. Trends Immunol. 2012;33(2):84-90.
32. Redeker A, Remmerswaal EBM, van der Gracht ETI, Welten SPM, Hollt T, Koning F, et al. The Contribution of Cytomegalovirus Infection to Immune Senescence Is Set by the Infectious Dose. Front Immunol. 2017;8:1953.
33. Davies B, Prier JE, Jones CM, Gebhardt T, Carbone FR, Mackay LK. Cutting Edge: Tissue-Resident Memory T Cells Generated by Multiple Immunizations or Localized Deposition Provide Enhanced Immunity. J Immunol. 2017;198(6):2233-7.
34. Holz LE, Chua YC, de Menezes MN, Anderson RJ, Draper SL, Compton BJ, et al. Glycolipid-peptide vaccination induces liver-resident memory CD8+ T cells that protect against rodent malaria. Science immunology. 2020;5(48):eaaz8035.
35. Panagioti E, Redeker A, van Duikeren S, Franken KL, Drijfhout JW, van der Burg SH, et al. The Breadth of Synthetic Long Peptide Vaccine-Induced CD8+ T Cell Responses Determines the Efficacy against Mouse Cytomegalovirus Infection. PLoS Pathog. 2016;12(9):e1005895.
36. Zwaveling S, Mota SCF, Nouta J, Johnson M, Lipford GB, Offringa R, et al. Established Human Papillomavirus Type 16-Expressing Tumors Are Effectively Eradicated Following Vaccination with Long Peptides. The Journal of Immunology. 2002;169(1):350-8.
37. van Duikeren S, Fransen MF, Redeker A, Wieles B, Platenburg G, Krebber WJ, et al. Vaccine-induced effector-memory CD8+ T cell responses predict therapeutic efficacy against tumors. J Immunol. 2012;189(7):3397-403.
38. Zom GG, Willems M, Khan S, van der Sluis TC, Kleinovink JW, Camps MGM, et al. Novel TLR2-binding adjuvant induces enhanced T cell responses and tumor eradication. J Immunother Cancer. 2018;6(1):146.

39. Panagioti E, Boon L, Arens R, van der Burg SH. Enforced OX40 Stimulation Empowers Booster Vaccines to Induce Effective CD4+ and CD8+ T Cell Responses against Mouse Cytomegalovirus Infection. Frontiers in Immunology. 2017;8(144).
40. van der Sluis TC, van Duikeren S, Huppelschoten S, Jordanova ES, Beyranvand Nejad E, Sloots A, et al. Vaccine-induced tumor necrosis factor-producing T cells synergize with cisplatin to promote tumor cell death. Clin Cancer Res. 2015;21(4):781-94.
41. van der Gracht ETI, Behr FM, Arens R. Functional Heterogeneity and Therapeutic Targeting of Tissue-Resident Memory T Cells. Cells. 2021;10(1).

Supplementary information

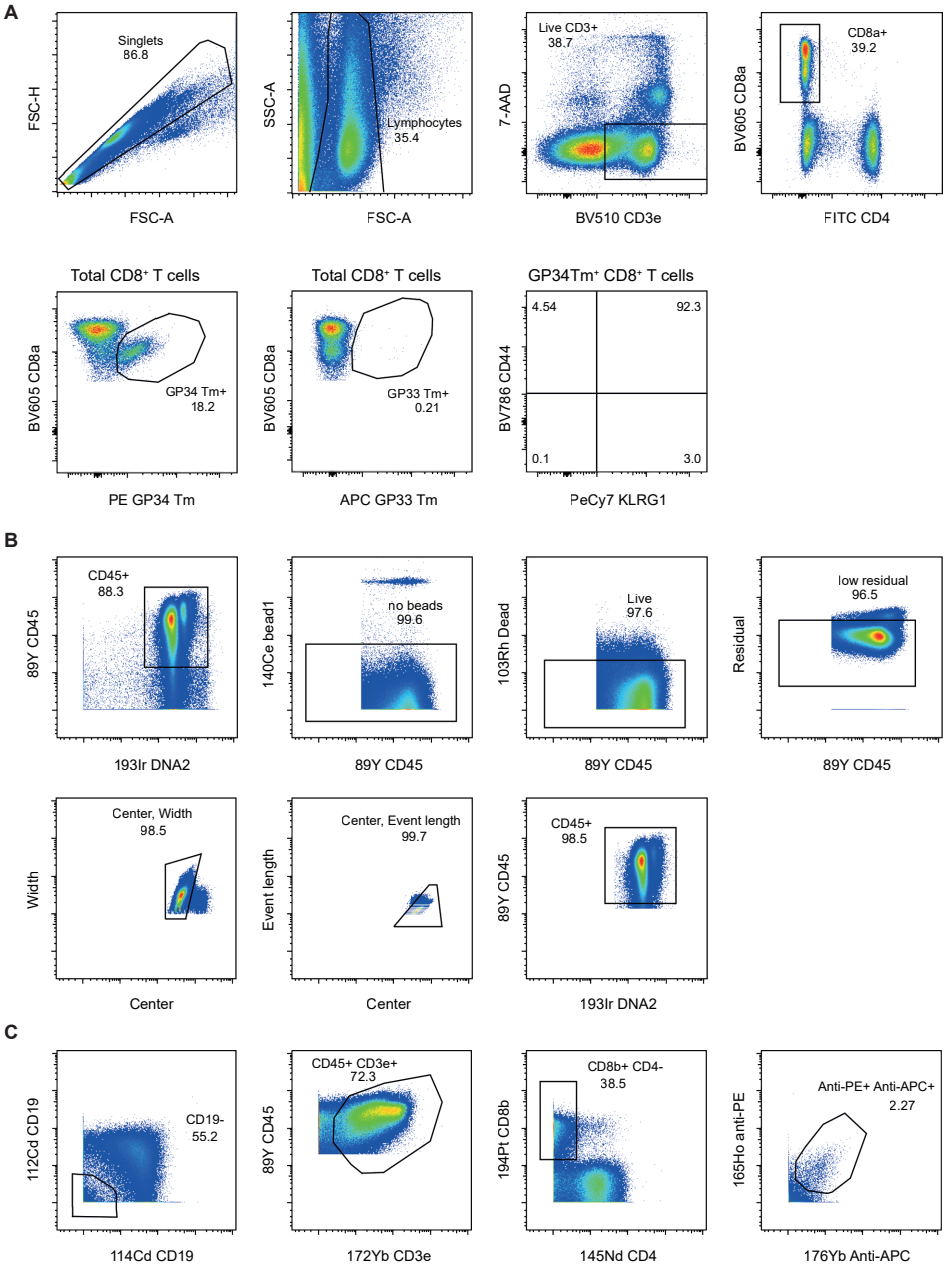

Figure S1. Gating strategy flow cytometry and mass cytometry. Related to Figure 1 and Figure 3. A) C57BL/6 mice were vaccinated with 100ug GP34 SLP + 20ug CpG 3 times in a prime-boost-boost setting with 2 week intervals. Representative plots show the gating strategy of detecting GP34-specific CD8⁺ T cells (depicted in Figure 1B) taken from blood and analyzed by flow cytometry. No GP33-specific CD8⁺ T cells (epitope $GP_{33\text{-}41}$ (KAVYNFATC)) were present upon GP34 vaccination. B,C) Representative plots show the gating strategy of CD45⁺ live cells (B) and GP34-specific CD8⁺ T cells (C) obtained from the liver and analyzed by mass cytometry.

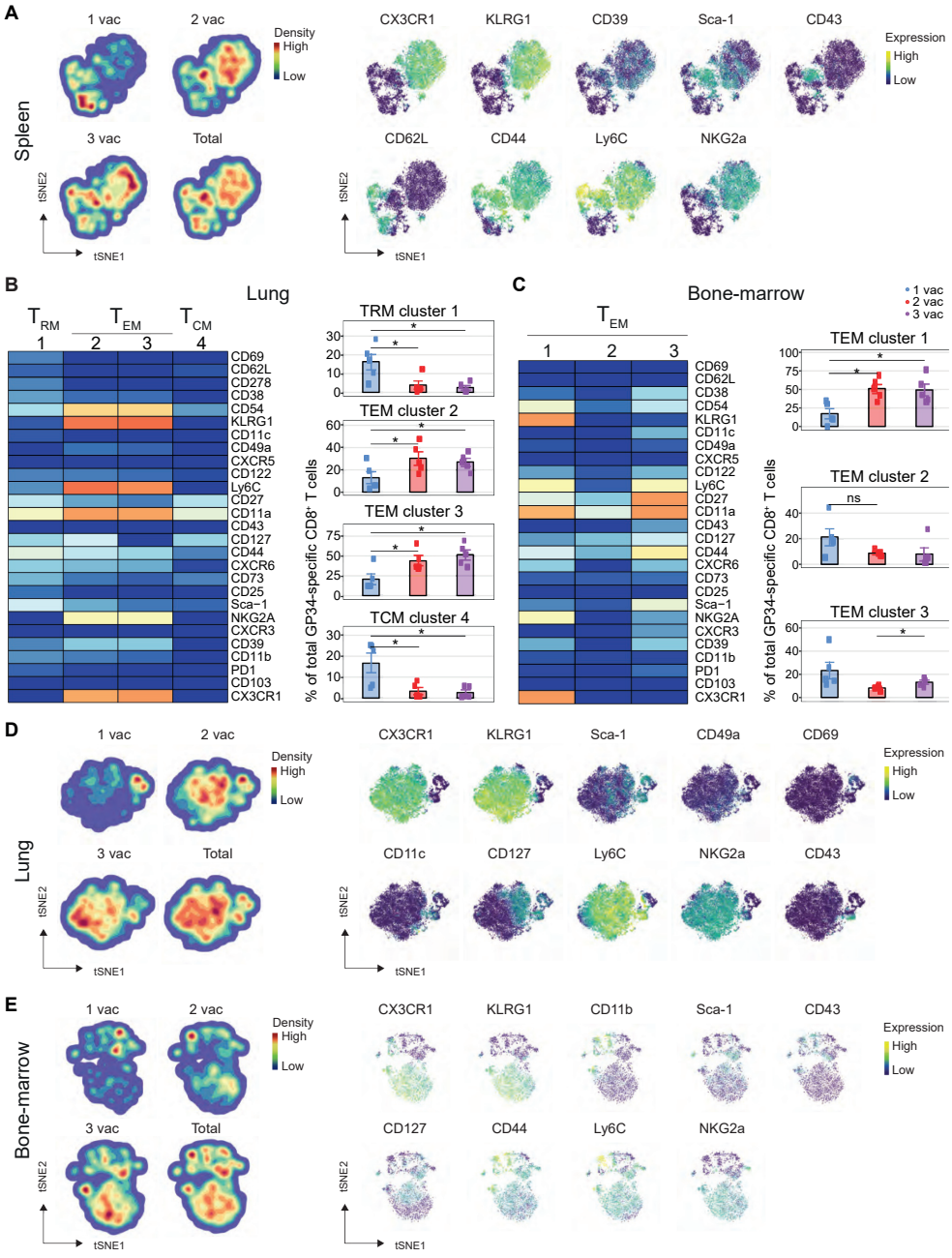
A
Spleen
1 vac
2 vac
3 vac
Total
Density
High
Low
tSNE2
tSNE1
CX3CR1
KLRG1
CD39
Sca-1
CD43
CD62L
CD44
Ly6C
NKG2a
Expression
High
Low
B
Lung
T_RM
T_EM
T_CM
1
2
3
4
CD69
CD62L
CD278
CD38
CD54
KLRG1
CD11c
CD49a
CXCR5
CD122
Ly6C
CD27
CD11a
CD43
CD127
CD44
CXCR6
CD73
CD25
Sca−1
NKG2A
CXCR3
CD39
CD11b
PD1
CD103
CX3CR1
TRM cluster 1
TEM cluster 2
TEM cluster 3
TCM cluster 4
% of total GP34-specific CD8+ T cells
C
Bone-marrow
T_EM
1 vac
2 vac
3 vac
TEM cluster 1
TEM cluster 2
TEM cluster 3
ns
D
Lung
CD49a
CD69
CD11c
CD127
E
Bone-marrow

Figure S2. Heterogeneity of antigen-specific CD8+ T cells in lung and bone-marrow. Related to Figure 4. A) tSNE embeddings of spleen GP34-specific CD8+ T cells isolated from vaccinated mice. Distribution of GP34-specific CD8+ T cells per vaccination in one tSNE analysis. Expression intensity of the cell-surface markers on the GP34-specific CD8+ T cells. The color of the cells indicates ArcSinh5-transformed expression values for a given marker analyzed. B, C) Mass cytometry data of GP34-specific CD8+ T cells in the lung (B) and bone marrow (C) of mice that received sequential vaccinations. Level of ArcSinh5transformed expression marker is displayed by a rainbow scale. Average and SEM in percentage of each CD8+ T cell cluster among the GP34-specific CD8+ T-cell population of one vaccination (blue bars), two vaccinations (red bars) and three vaccinations (purple bars). D, E) tSNE embeddings of lung (D) and bone-marrow (E) GP34-specific CD8+ T cells isolated from vaccinated mice. Distribution of GP34-specific CD8+ T cells per vaccination in one tSNE analysis. Expression intensity of the cell-surface markers on the GP34-specific CD8+ T cells. The color of the cells indicates ArcSinh5-transformed expression values for a given marker analyzed.

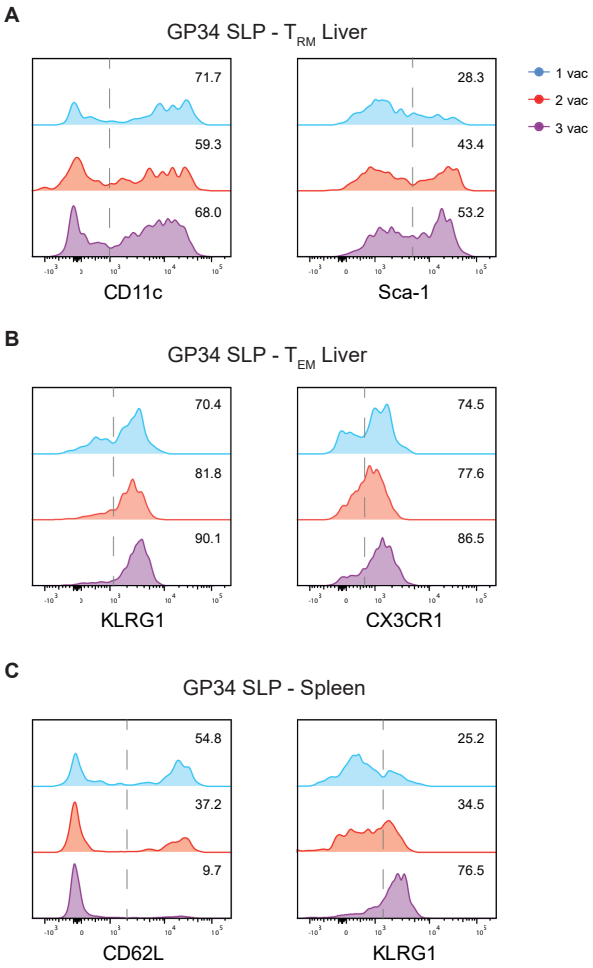

Figure S3. Phenotype of antigen-specific CD8⁺ T cells upon booster vaccination. Related to Figure 4. A, B) Flow cytometry data showing the phenotype of antigen-specific CD69⁺ T_{RM} cells (A) and antigen-specific CD69⁻ T cells (B) in liver around 60 days after 1, 2 or 3 times GP34 SLP vaccination in a prime-boost-boost setting. Indicated the percentage of positive cells. C) Flow cytometry data showing the phenotype of antigen-specific CD8⁺ T cells in spleen around 60 days after 1, 2 or 3 times GP34 SLP vaccination in a prime-boost-boost setting. Indicated the percentage of positive cells.

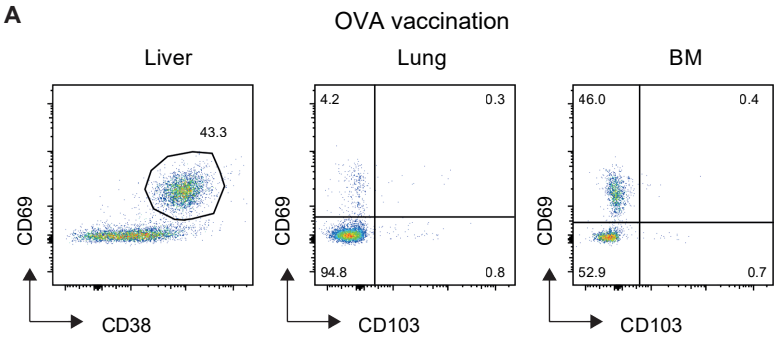

Figure S4. OVA SLP vaccination induces antigen-specific CD8⁺ T_{RM} cells in multiple organs. Related to Figure 5. A,B) Presence of antigen-specific CD8⁺ T_{RM} cells in liver, lung and bone-marrow upon 3 vaccinations, day 50 after the first OVA SLP vaccination. Mice were vaccinated s.c. with SLP (100ug) + CpG (20ug) in a prime-boost-boost setting with 2 week intervals.

Table S1. CyTOF Mass Cytometry Panel. Anti-mouse monoclonal antibodies used for staining of cells for mass cytometry analysis. Antibodies were either purchased pre-conjugated, or antibodies were conjugated to the indicated lanthanide metal isotopes.

Antibody	Clone	Metal	Pre-conjugated	Company	Cat no	Cat no metal (Fluidigm)
Anti-PE	PE001	165 Ho	x	Fluidigm	3165015B	
Anti-APC	APC003	176 Yb	x	Fluidigm	3176007B	
CD3e	145-2C11	172 Yb		eBioscience	14-0031-86	201172A
CD4	RM4-5	145 Nd	x	Fluidigm	3145002B	
CD8a	53-6.7	168 Er	x	Fluidigm	3168003B	
CD8b	YTS156.7.7	194 Pt		BioLegend	126602	201194
CD11a	M17/4	160 Gd		eBioscience	16-0111-82	201160A
CD11b	M1/70	154 Sm	x	Fluidigm	3154006B	
CD11c	N418	167 Er		eBioscience	14-0114-85	201167A
CD19	6D5	Qdot655: 112/114 Cd	x	ThermoFisher	Q10379	
CD25	3C7	150 Nd	x	Fluidigm	3150002B	
CD27	LG.3A10	158 Gd		eBioscience	14-0272-82	201158A
CD38	90	163 Dy		eBioscience	14-0381-85	201163A
CD39	24DMS1	152 Sm		eBioscience	14-0391-82	201152A
CD43	1B11	115 In		BioLegend	121202	
CD44	IM7	142 Nd		eBioscience	14-0441-86	201142A
CD45	30-F11	89Y	x	Fluidigm	3089005B	
CD49a	Ha31/8	151 Eu		BD Biosciences	555001	201151A
CD54	YN1/1.7.4	164 Dy		BioLegend	116102	201164A
CD62L	MEL-14	169 Tm		BioLegend	104443	201169A
CD69	H1.2F3	143 Nd	x	Fluidigm	3143004B	
CD73	TY/23	148 Nd		BD Biosciences	550738	201148A
CD86	GL1	171 Yb		eBioscience	14-0862-85	201171A
CD103	2.E7	173 Yb		eBioscience	14-1031-85	201173A
CD122	TM-b1	155 Gd		eBioscience	14-1222-85	201155A
CD127	A7R34	175 Lu	x	Fluidigm	3175006B	
CD160	7H1	209 Bi		BioLegend	143002	
CD161	PK136	170 Er	x	Fluidigm	3170002B	
CD223	eBioC9B7W	161 Dy		eBioscience	14-2231-85	201161A
CD278	7E.17G9	162 Dy		eBioscience	14-9942-85	201162A
CX3CR1	SA011F11	174 Yb		BioLegend	149002	201174A
CXCR3	CXCR3-173	149 Sm		eBioscience	16-1831-85	201149A
CXCR5	L138D7	153 Eu		BioLegend	145502	201153A
CXCR6	SA051D1	144 Nd		BioLegend	151102	201144A
FR4	TH6	198 Pt		BioLegend	125102	201198
KLRG1	2F1	166 Er		eBioscience	16-5893-85	201166A
Ly6C	HK1.4	156 Gd		eBioscience	16-5932-85	201156A
NKG2A	20d5	147 Sm		eBioscience	16-5896-85	201147A
PD-1	29F.1A12	159 Tb	x	Fluidigm	3159024B	
Sca-1	D7	141 Pr		BioLegend	108135	201141A
TCRgd	eBioGL3	146 Nd		eBioscience	14-5711-85	201146A